

Holographic polytropic $f(T)$ -gravity models

Surajit Chattopadhyay,^{1,*} Abdul Jawad,^{2,†} and Shamaila Rani^{2,‡}

¹ *Pailan College of Management and Technology,
Bengal Pailan Park, Kolkata-700 104, India.*

² *Department of Mathematics, COMSATS Institute of
Information Technology, Lahore-54000, Pakistan.*

(Dated: October 7, 2015)

The present paper reports a study on the cosmological consequences arising from reconstructing $f(T)$ gravity through new holographic-polytropic dark energy. We assume two approaches, namely a particular form of Hubble parameter H and a solution for $f(T)$. We obtain the deceleration parameter, effective equation of state as well as torsion equation of state parameters from total density and pressure in both cases. It is interesting to mention here that the deceleration and torsion equation of state represent transition from deceleration to acceleration phase. We study the statefinder parameters under both approaches which result that statefinder trajectories are found to attain Λ CDM point. The comparison with observational data represents consistent results. Also, we discuss the stability of reconstructed models through squared speed of sound which represents stability in late times.

PACS numbers: 98.80.-k; 04.50.Kd

I. INTRODUCTION

The accelerated expansion of the universe is strongly manifested after the discovery of unexpected reduction in the detected energy fluxes coming from SNe Ia [1, 2]. Other observational data like CMBR, LSS and galaxy redshift surveys [3–5] also provide evidences in this favor. These observations propose a mysterious form of force, referred as dark energy (DE), reviewed in [6–9], which takes part in the expansion phenomenon and dominates overall energy density of the universe. This has two remarkable features: its pressure must be negative in order to cause the cosmic acceleration and it does not cluster at large scales. In spite of solid favor about the presence of DE from the observations, its unknown nature is the biggest puzzle in astronomy. In the last nineties,

*Electronic address: surajitchatto@outlook.com, surajcha@iucaa.ernet.in

†Electronic address: abduljawad@ciitlahore.edu.pk, jawadab181@yahoo.com

‡Electronic address: drshamailarani@ciitlahore.edu.pk, shamailatoor.math@yahoo.com

this expansion was detected but the evidence for DE has been developed during the past decade.

Physical origin of DE is one of the largest mysteries not only in cosmology but also in fundamental physics [6, 10–13]. The dynamical nature of DE can be originated from different models such as cosmological constant, scalar field models, holographic DE (HDE), Chayplygin gas, polytropic gas and modified gravity theories. Various DE models are discussed in the references [14–21]. The modified theories of gravity are the generalized models came into being by modifying gravitational part in general relativity (GR) action while matter part remains unchanged. At large distances, these modified theories, modify the dynamics of the universe. The $f(R)$ theory is the modification of GR which modifies the Ricci (curvature) scalar R to a general differentiable function. The gravitational interaction is established through curvature with the help of Levi-Civita connection. There is another theory which is the result of unification of gravitation and electromagnetism. It is based on mathematical structure of absolute or distant parallelism, also referred as teleparallelism which led to teleparallel gravity. In this gravity, torsion is used as the gravitational field via Wittenböck connection. The modification of teleparallel gravity in the similar fashion of $f(R)$ gravity gives generalized teleparallel gravity, $f(T)$ gravity where f is general differentiable function of torsion scalar.

The search for a viable DE model (representing accelerated expansion of the universe) is the basic key leading to the reconstruction phenomenon, particularly in modified theories of gravity [22–25]. This reconstruction scheme works on the idea of comparison of corresponding energy densities to obtain the modified function in the underlying gravity. Daouda et al. [29] developed the reconstruction scheme via HDE model in $f(T)$ gravity and found that the reconstructed model may cross the phantom divide line in future era. Setare and Darabi [30] assumed the scale factors in power-law form and obtained well defined solutions. Farooq et al. [34] reconstructed $f(T)$ model by taking (m, n) –type HDE model and discussed its viability as well as cosmography. They showed that this model is viable, compatible with solar system test, ghost-free and has positive gravitational constant. Karami and Abdolmaleki [35] obtained equation of state (EoS) parameter for the reconstructed $f(T)$ models by taking HDE, new agegraphic DE as well as their entropy-corrected versions and found transition from non-phantom to phantom phase only in entropy-corrected versions showing compatibility with the recent observations. Sharif and Rani [36, 37] explored this theory via some scalar fields, nonlinear electrodynamics and entropy-corrected HDE models and analyze the accelerated expansion of the universe.

Holographic DE models are widely used for explaining the present day DE scenario and evolution of the universe. These are based on the holographic principle which naively asks that the

combination of quantum mechanics and quantum gravity requires three-dimensional world to be an image of data that can be stored on a two-dimensional projection much like a holographic image [38, 39]. It is useful to reveal the entropy bounds of black holes (BHs) which lead to the formulation of the holographic principle. It is well established that the area of a BH event horizon never decreases with time so called area theorem. If a matter undergoes gravitational collapse and converts into a BH, the entropy associated with the original system seems to disappear since the final state is unique. This process clearly violates the second law of thermodynamics. In order to avoid this problem, Bekenstein [40] proposed generalized second law of thermodynamics on the basis of area theorem which is stated as, BH carries an entropy proportional to its horizon area and that the total entropy of ordinary matter system and BH never decreases. Mathematically, it can be written as

$$\frac{dS_{tot}}{dt} \geq 0. \quad (1)$$

Here $S_{tot} = S + S_{BH}$, S represents the entropy of matter (body) outside a BH and S_{BH} is the entropy of BH.

In the construction of HDE model, the relation between ultra-violet (UV) (Λ) and infra-red (IR) (L) cutoffs as proposed by Cohen et al. [41] plays a key role. It is suggested that for an effective field theory in a box of size L with Λ , the entropy S scales extensively, i.e., $S \sim L^3 \Lambda^3$. However, the maximum entropy in a box possessing volume L^3 (growing with the area of the box) behaves non-extensively in the framework of BH thermodynamics so called Bekenstein entropy bound. For any Λ (containing sufficiently large volume), the entropy of effective field theory will exceed the Bekenstein limit which can be satisfied if we limit the volume of the system as follows

$$S = L^3 \Lambda^3 \lesssim S_{BH} \equiv \pi L^2 M_p^2, \quad (2)$$

where S_{BH} has radius L .

It can be seen from the above inequality that IR cutoff L (scales as Λ^{-3}) is directly associated with UV cutoff and cannot be chosen independently from it. Moreover, there occur some problems in saturating the above inequality because Schwarzschild radius is much larger than the box size and hence produces incompatibility problem with effective field theory. To avoid this problem, Cohen et al. [41] proposed a strong constraint on the IR cutoff which excludes all states that lie within the Schwarzschild radius, i.e.,

$$L^3 \Lambda^4 = L^3 \rho_\Lambda \lesssim L M_p^2. \quad (3)$$

Here, left and right hand sides correspond to the total energy of the system (since the maximum energy density in the effective field theory is Λ^4) and mass of the Schwarzschild BH, respectively. Also, IR cutoff L is being scaled as Λ^{-2} which is more restrictive limit than (2). The above relation indicates that the maximum entropy of the system will be $S_{BH}^{\frac{3}{4}}$. Li [42] developed the energy density for DE model by saturating the above inequality as follows

$$\rho_\Lambda = 3\zeta^2 M_p^2 L^{-2}, \quad (4)$$

where ζ is the dimensionless HDE constant parameter. The interesting feature of this density is that it provides a relation between UV (bound of vacuum energy density) and IR (size of the universe) cutoffs. However, a controversy about the selection of IR cutoff of HDE has been raised since its birth. As a result, different proposals of IR cutoffs for HDE and its entropy corrected versions [43] have been developed.

Plan of the paper is as follows: In section II, we provide briefly about holographical polytropic DE model and some cosmological parameters. In IIA, we assume a particular form of Hubble parameter and subsequently considering a correspondence between new HDE and polytropic gas model of DE derived a new form of polytropic gas dark energy that was further assumed to be an effective description of dark energy in $f(T)$ gravity to study the cosmological consequences. In section IIB we assume a particular solution for $f(T)$ and derive solution for H in the backdrop of a correspondence between new HDE and polytropic DE. This reconstructed H has been utilized to get reconstructed effective torsion EoS and statefinder parameters. Also, we compare the obtained results with observational data in section IIC. In the next section III, we check the stability of reconstructed models in all cases. We conclude the results in section VI.

II. NEW HOLOGRAPHIC POLYTROPIC DE IN $f(T)$ GRAVITY

Holographic reconstruction of modified gravity model is a very active area of research in cosmology. Unfortunately, nature of DE is still not known and probably that has motivated theoretical physicists towards development of various candidates of DE and recently geometric DE or modified gravity has been proposed as a second approach to account for the late time acceleration of the universe. In literature, mostly reconstructed work has been done with polytropic EoS, family of holographic DE models, family of Chaplygin gas, scalar field models in general relativity as well as modified theories of gravity (in framework of $f(T)$ gravity, see [29, 30, 34–37]–[44–46]). However, we do holographically reconstruction of polytropic DE and based on that we experiment with the

cosmological implications of $f(T)$ gravity.

The polytropic gas model can explain the EoS of degenerate white dwarfs, neutron stars and also the EoS of main sequence stars. Polytropic gas EoS is given by [51]

$$p_\Lambda = K \rho_\Lambda^{1+\frac{1}{n}}, \quad (5)$$

where K is a positive constant and n is the polytropic index. The important role played by polytropic EoS in astrophysics has been emphasized in [51, 52]. It is a simple example which is nevertheless not too dissimilar from realistic models [51]. Moreover, there are cases where a polytropic EoS is a good approximation to reality [51]. From continuity equation

$$\rho_\Lambda = \left(\frac{1}{Ba^{\frac{3}{n}} - K} \right)^n. \quad (6)$$

In the present work, we are considering a correspondence between polytropic DE and new HDE with an IR cut-off proposed by [53] with the density given by

$$\rho_D = 3(\mu\dot{H} + \nu H^2). \quad (7)$$

Statefinder and Cosmographic Parameters

Some cosmological parameters are very important for describing the geometry of the universe which include EoS, parameter, deceleration parameter and statefinder etc. The physical state of a homogenous substance can be described by EoS. This state is associated with the matter including pressure, temperature, volume and internal energy. It can be defined in the form $p = p(\rho, \hat{T})$, where ρ , p and \hat{T} are the mass density, isotropic pressure and absolute temperature, respectively. In cosmological context, EoS is the relation between energy density and pressure such as $p = p(\rho)$ and is given by

$$p = \omega \rho, \quad (8)$$

where ω represents the dimensionless EoS parameter which helps to classify different phases of the universe.

In order to differentiate different DE models on behalf of their role in explaining the current status of the universe, Sahni et al. [47] proposed statefinder parameters. These are denoted by (r, s) and are defined in terms of Hubble as well as deceleration parameters. The deceleration parameter is defined as

$$q = -\frac{\ddot{a}}{aH^2} = -\left(1 + \frac{\dot{H}}{H^2}\right). \quad (9)$$

The negative value of this parameter represents the accelerated expansion of the universe due to the term $\ddot{a} > 0$ (indicating expansion with acceleration). The statefinder parameters are given by

$$r = \frac{\ddot{a}}{aH^3}, \quad s = \frac{r-1}{3(q-\frac{1}{2})}. \quad (10)$$

These parameters possess geometrical diagnostic because of their total dependence on the expansion factor. The most remarkable feature of (r, s) plane is that we can find the distance of a given DE model from Λ CDM limit. This depicts the well-known regions given as follows:

- (i) $(r, s) = (1, 0)$ shows Λ CDM limit;
- (ii) $(r, s) = (1, 1)$ describes CDM limit;
- (iii) $r < 1$ and $s > 0$ constitute quintessence and phantom DE regions.

Moreover, r can be expressed in terms of deceleration parameter as

$$r = 2q^2 + q - \frac{\dot{q}}{H}. \quad (11)$$

Both H and $\{r, s\}$ are categorized as cosmographic parameters. The cosmographic parameters, being dependent on the only stringent assumption of homogeneous and isotropic universe, marginally depend on the choice of a given cosmological model. Secondly, cosmography alleviates degeneracy, because it bounds only cosmological quantities which do not strictly depend on a model. The cosmographic set of parameters arising out of Taylor series expansion of $a(t)$ around the present epoch can be summarized as [48, 49]

$$\begin{aligned} H &= \frac{1}{a} \frac{da}{dt}; & q &= -\frac{1}{aH^2} \frac{d^2a}{dt^2} \\ j &= \frac{1}{aH^3} \frac{d^3a}{dt^3}; & s &= \frac{1}{aH^4} \frac{d^4a}{dt^4} \end{aligned} \quad (12)$$

Differentiating Friedman equation with respect to t and using Eq. 12 one can write

$$\dot{H} = -H^2(1 + q) \quad (13)$$

$$\ddot{H} = H^3(j + 3q + 2) \quad (14)$$

$$\ddot{\ddot{H}} = H^4(s - 4j - 3q(q + 4) - 6) \quad (15)$$

In the context of cosmological reconstruction problem, some notable contributions are [55–57]. It may be noted that the present work is motivated by Karami and Abdolmaleki [35].

A. With a specific choice of H

We consider that the Hubble rate H is given by [54]

$$H = H_0 + \frac{H_1}{t}, \quad (16)$$

leading to

$$a(t) = C_1 e^{H_0 t} t^{H_1}. \quad (17)$$

Due to this choice of Hubble parameter, the EoS takes the form

$$w_\Lambda = -1 + \frac{B (C_1 e^{H_0 t} t^{H_1})^{\frac{1}{n}}}{-K + B (C_1 e^{H_0 t} t^{H_1})^{\frac{1}{n}}}, \quad (18)$$

and subsequently NHDE density becomes

$$\rho_D = 3 \left(-\frac{H_1 \mu}{t^2} + \left(H_0 + \frac{H_1}{t} \right)^2 \nu \right). \quad (19)$$

From continuity equation we have

$$w_D = -1 - \frac{\frac{2H_1 \mu}{t^3} - \frac{2H_1 (H_0 + \frac{H_1}{t}) \nu}{t^2}}{3 (H_0 + \frac{H_1}{t}) \left(-\frac{H_1 \mu}{t^2} + (H_0 + \frac{H_1}{t})^2 \nu \right)}. \quad (20)$$

Considering a correspondence between polytropic DE and new HDE i.e. $\rho_\Lambda = \rho_D$ and $w_\Lambda = w_D$ we express B and K in terms of a in the following arrangement

$$B = \frac{23^{-\frac{1+n}{n}} H_1 (C_1 e^{H_0 t} t^{H_1})^{-1/n} (-\mu + (H_1 + H_0 t) \nu) \left(\frac{t^2}{-H_1 \mu + (H_1 + H_0 t)^2 \nu} \right)^{1+\frac{1}{n}}}{t^2 (H_1 + H_0 t)} \quad (21)$$

$$K = 3^{-\frac{1+n}{n}} \left(\frac{t^2}{-H_1 \mu + (H_1 + H_0 t)^2 \nu} \right)^{\frac{1}{n}} \left(-3 + \frac{2}{H_1 + H_0 t} - \frac{2H_0 t \nu}{-H_1 \mu + (H_1 + H_0 t)^2 \nu} \right). \quad (22)$$

It may be noted that B and K being integration constants they are not functions of a . Rather it is a new arrangement arising out of consideration of a correspondence between new holographic dark energy and polytropic gas dark energy. Using Eqs. (21) and (22) in Eq. (6) we get the new holographic-polytropic gas density as

$$\rho_\Lambda = 3 \left(\frac{t^2}{-H_1 \mu + (H_1 + H_0 t)^2 \nu} \right)^{-1} \quad (23)$$

The modified Friedmann equations in the case of $f(T)$ gravity for the spatially flat FRW universe are given by

$$H^2 = \frac{1}{3} (\rho_m + \rho_T), \quad (24)$$

$$2\dot{H} + 3H^2 = -(\rho_m + p_T), \quad (25)$$

where

$$\rho_T = \frac{1}{2} (2T f_T - f - T), \quad (26)$$

$$p_T = -\frac{1}{2} \left[-8\dot{H} f_{TT} + (2T - 4\dot{H}) f_T - f + 4\dot{H} - T \right], \quad (27)$$

$$T = -6H^2. \quad (28)$$

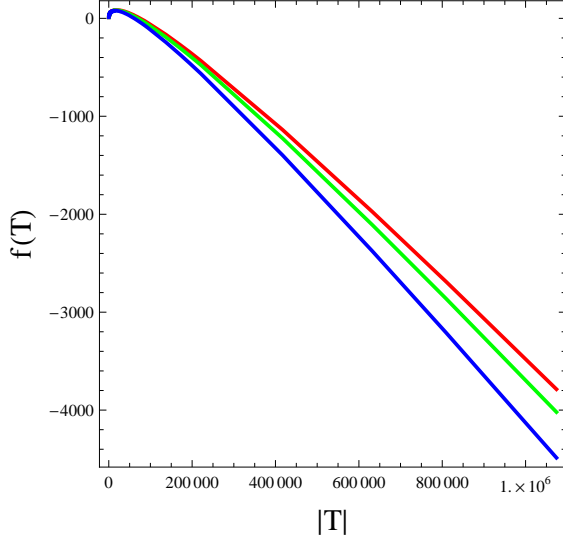


FIG. 1: Reconstructed $f(T)$ (Eq. (37)) and we see that $f(T) \rightarrow 0$ as $T \rightarrow 0$.

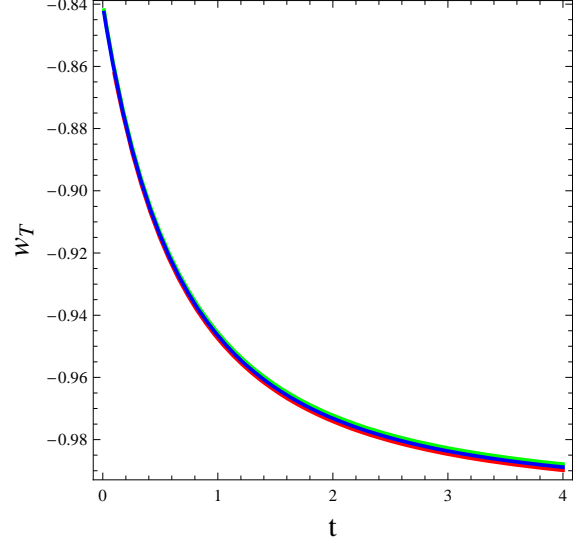


FIG. 2: Effective torsion EoS parameter as in Eq. (38).

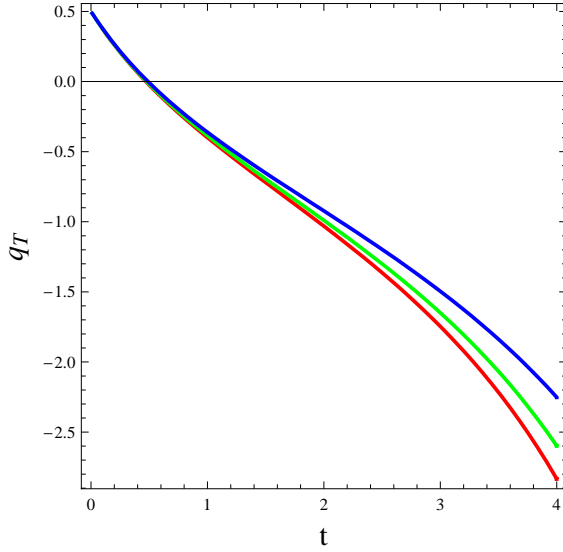


FIG. 3: Deceleration parameter as in Eq. (39).

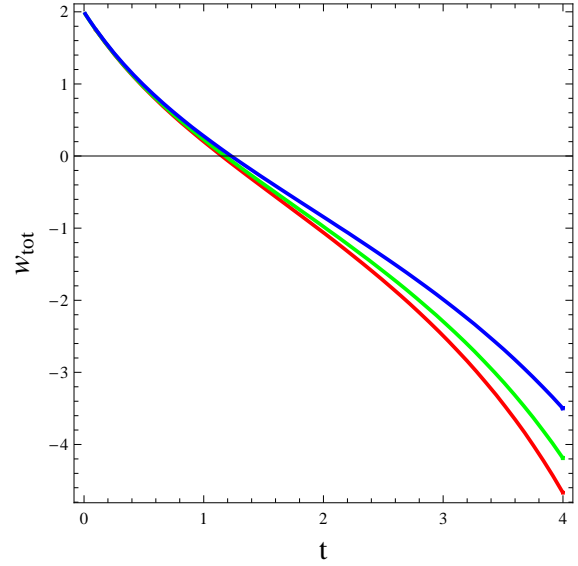


FIG. 4: Plot of w_{tot} as in Eq. (43).

Here ρ_m and p_m are the energy density and pressure of matter inside the universe, respectively. Also ρ_T and p_T are the torsion contributions to the energy density and pressure. The energy conservation laws are given by

$$\dot{\rho}_T + 3H(\rho_T + p_T) = 0, \quad (29)$$

$$\rho_m + 3H(\rho_m + p_m) = 0. \quad (30)$$

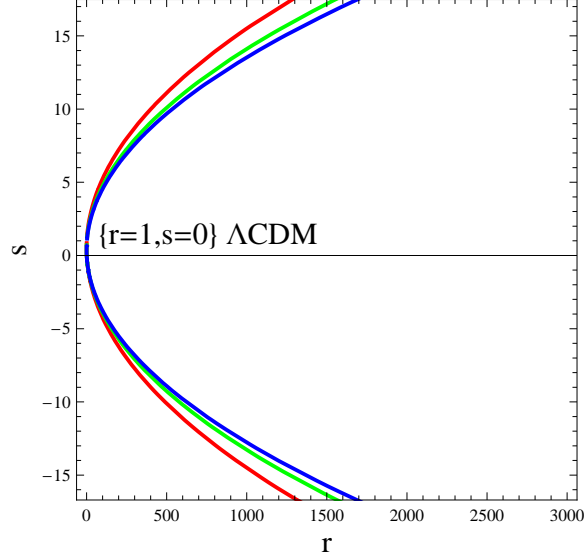


FIG. 5: Statefinder parameters for the choice of $H = H_0 + \frac{H_1}{t}$.

Using Eqs. (26) and (27), the effective torsion EoS parameter comes out to be

$$w_T = -1 + \frac{4\dot{H}(2Tf_{TT} + f_T - 1)}{2Tf_T - f - T}, \quad (31)$$

Using Eqs. (24), (26) and (28) one can get

$$\rho_m = \frac{1}{2}(f - 2Tf_T) \quad (32)$$

The deceleration parameter

$$q_T = 2 \left(\frac{f_T - T f_{TT} - \frac{3f}{4T}}{f_T + 2T f_{TT}} \right) \quad (33)$$

The dark torsion contribution in $f(T)$ gravity can justify the observed acceleration of the universe without resorting to DE. This motivates us to reconstruct an $f(T)$ -gravity model according to the new holographic-polytropic DE. Considering $\rho_T = \rho_\Lambda$ i.e. equating Eqs. (23) and (26) we have the following differential equation

$$6 \left(H_0 + \frac{H_1}{t} \right)^2 - f - \frac{t^2}{H_1} \left(H_0 + \frac{H_1}{t} \right) \frac{df}{dt} = 6 \left(\frac{t^2}{-\mu H_1 + (H_0 t + H_1)^2 \nu} \right)^{-1}. \quad (34)$$

Solving (34), we obtain reconstructed f in terms of cosmic time t

$$f(t) = \frac{1}{H_1 t^2} \left[H_1 \left\{ H_0 t (C_2 t - 12\mu) + H_1 (C_2 t - 6\mu + 6H_0 t(-1 + \nu)) + 6H_1^2(-1 + \nu) \right\} + 12H_0 t (H_1 + H_0 t) \mu \ln \left(\frac{H_1}{t} + H_0 \right) \right]. \quad (35)$$

Considering $H = (-\frac{T}{6})^{1/2}$, we have

$$t = \frac{6H_1}{-6H_0 + \sqrt{-6T}}, \quad (36)$$

that lead to re-expressing f of (35) as a function of T as

$$f(T) = \frac{C_2 H_1 \sqrt{-6T} + 6(6H_0^2 \mu - H_0 H_1 \sqrt{-6T}(-1 + \nu) + T(H_1 + \mu - H_1 \nu)) + 6H_0 \sqrt{-6T} \mu \ln \left[-\frac{T}{6}\right]}{6H_1}. \quad (37)$$

Subsequently using (37) in (31) and (33), we get the effective torsion EoS and deceleration parameters as

$$w_T = -1 + \frac{(-6H_0 + \sqrt{-6T})^2 (6H_0 \mu + \sqrt{-6T}(-\mu + H_1 \nu))}{9\sqrt{-6T} H_1 (-6H_0^2 \mu + 2\sqrt{-6T} H_0 \mu + T(\mu - H_1 \nu))}, \quad (38)$$

and

$$q_T = \frac{-(-18H_0^2 + 4\sqrt{-6T} H_0 + T) \mu + H_1 T(-1 + \nu)}{-2(H_0 \sqrt{-6T} + T) \mu + 2H_1 T(-1 + \nu)}, \quad (39)$$

Using Eq. (37) in (32) density of the dark matter inside the universe becomes

$$\rho_m = \frac{(6H_0^2 - 2\sqrt{-6T} H_0 - T) \mu + H_1 T(-1 + \nu)}{2H_1}. \quad (40)$$

In the case of pressureless dust matter, $p_m = 0$, we obtain

$$\dot{H} = -\frac{1}{2} \left(\frac{\rho_m}{f_T + 2T f_{TT}} \right). \quad (41)$$

Using Eqs. (37) and (40) in (41) we get

$$\dot{H} = \frac{\sqrt{\frac{-3T}{2}} (2H_0 (-3H_0 + \sqrt{-6T}) \mu + T(H_1(1 - \nu) + \mu))}{2(-6H_0 \mu + \sqrt{-6T}(H_1(1 - \nu) + \mu))}. \quad (42)$$

Defining the effective energy-density and pressure as $\rho_{tot} = \rho_T + \rho_m$ and $p_{tot} = p_T$ ($p_m = 0$) the effective EoS $w_{tot} = p_{tot}/\rho_{tot}$ becomes (using Eq. (42))

$$w_{tot} = -1 - \frac{2\dot{H}}{3H^2} = -1 - \frac{3\sqrt{6} (2H_0 (-3H_0 + \sqrt{-6T}) \mu + T(H_1(1 - \nu) + \mu))}{6H_0 \sqrt{-T} \mu + \sqrt{6T}(H_1(1 - \nu) + \mu)}. \quad (43)$$

The statefinder parameters are given by

$$r = q + 2q^2 + \frac{\dot{q}}{H} \quad (44)$$

$$s = \frac{r - 1}{3(q - \frac{1}{2})}. \quad (45)$$

In the current framework Eq.(44) and (45) take the form

$$\begin{aligned} r = & -\frac{1}{H_1 T^2 (-6H_0 \mu + \sqrt{-6T}(H_1 + \mu - H_1 \nu))^2} \times \\ & 3(-3H_0 (36\sqrt{6}H_0^4 \sqrt{-T} + 36\sqrt{6}H_0^2 (-T)^{3/2} + \sqrt{6}(-T)^{5/2} + 144H_0^3 T - 24H_0 T^2) \mu^2 - \\ & H_1^2 T^2 (-54H_0^2 + 13H_0 \sqrt{-6T} + 4T) \mu(-1 + \nu) + \\ & 2H_1^3 T^3 (-1 + \nu)^2 + H_1 T \mu (2T^2 \mu - 6H_0^2 T(29\mu + 12(-1 + \nu)) + 108H_0^4 (-2 + 3\mu + 2\nu) + \\ & H_0 \sqrt{-6T} T(-3 + 13\mu + 3\nu) - 18\sqrt{6}H_0^3 \sqrt{-T}(-5 + 9\mu + 5\nu))) \end{aligned} \quad (46)$$

$$s = \frac{1}{3H_1T(6H_0\mu + \sqrt{6}\sqrt{-T}(-H_1 - \mu + H_1\nu))} \times \\ [36H_0^3\mu + \sqrt{6}(-1 + 3H_1)\sqrt{-T}T(-H_1 - \mu + H_1\nu) + \\ 18H_0T(-\mu + H_1(-1 + 2\mu + \nu)) + 6\sqrt{6}H_0^2\sqrt{-T}(-3\mu + H_1(-2 + 3\mu + 2\nu))] \quad (47)$$

It may be noted that in the present and subsequent figures red, green and blue lines correspond to $n = 6, 8$ and 10 respectively. Figure 2 shows the evolution of the effective torsion EoS parameter w_T as a function of t . In this case $w_T > -1$ and it is running close to -1 , but it is not crossing -1 boundary. This indicates “quintessence” behavior. In later time $-6H_0 + \sqrt{-6T} \rightarrow 0$ (see Eq. (38)) and as a consequence $w_T \rightarrow -1$. A clear transition from $q > 0$ to $q < 0$ is apparent at $t \approx 0.5$ in Figure 3. This indicates transition from decelerated to accelerated phase of the universe. In Figure 4, it is observed that w_{tot} behaves differently from w_{eff} . The w_{tot} transits from > -1 i.e. quintessence to < -1 i.e. phantom at $t \approx 1$. Statefinder parameters as obtained in Eqs. (46) and (47) are plotted in Figure 5 and it is observed that the fixed point $\{r = 1, s = 0\}_{\Lambda CDM}$ is attainable and the $\{r - s\}$ trajectory goes beyond the ΛCDM . It is palpable that for finite r , we have $s \rightarrow -\infty$. This indicates that the holographic-polytropic $f(T)$ gravity interpolates between dust and ΛCDM phase of the universe. In this framework, the cosmographic parameter j (jerk) comes out to be

$$j = -\frac{7}{2} + \frac{2H_1}{(H_1 + H_0t)^3} + \frac{9H_0t\mu}{2(H_1 + H_0t)(H_1 + H_0t + \mu - (H_1 + H_0t)\nu)} \quad (48)$$

B. With specific form of f and without any assumption about H

Power-law model of Bengochea and Ferraro

In this section, we are not assuming any form of H or a . Rather we assume f as the power-law model of Bengochea and Ferraro [50]

$$f(T) = \alpha(-T)^b \quad (49)$$

where α and b are the two model parameters. Considering $\rho_\Lambda = \rho_D$ we have the following differential equation

$$\frac{\mu a}{2} \left(\frac{dH^2}{da} \right) + \nu H^2 = \frac{1}{3} \left(Ba^{1/n} - K \right)^{-n} \quad (50)$$

solving which we get

$$H^2 = a^{-\frac{2\nu}{\mu}} C_1 + \frac{\left(1 - \frac{a^{\frac{1}{n}} B}{K} \right)^n \left(a^{\frac{1}{n}} B - K \right)^{-n} {}_2F_1 \left[\frac{2n\nu}{\mu}, n, 1 + \frac{2n\nu}{\mu}, \frac{a^{\frac{1}{n}} B}{K} \right]}{3\nu} \quad (51)$$

that leads to

$$\dot{H} = \frac{-3a^{-\frac{2\nu}{\mu}} C_1 \nu + \left(a^{\frac{1}{n}} B - K\right)^{-n} \left(1 - \left(1 - \frac{a^{\frac{1}{n}} B}{K}\right)^n 2F1\left[\frac{2n\nu}{\mu}, n, 1 + \frac{2n\nu}{\mu}, \frac{a^{\frac{1}{n}} B}{K}\right]\right)}{3\mu} \quad (52)$$

Therefore, using $T = -6H^2$ in Eq. (49) and thereafter using (32) we have the dark matter density of the universe as a function of a as

$$\rho_m = \frac{1}{2}(1 - 2b)\alpha \left(6a^{-\frac{2\nu}{\mu}} C_1 + \frac{2\left(1 - \frac{a^{\frac{1}{n}} B}{K}\right)^n \left(a^{\frac{1}{n}} B - K\right)^{-n} 2F1\left[\frac{2n\nu}{\mu}, n, 1 + \frac{2n\nu}{\mu}, \frac{a^{\frac{1}{n}} B}{K}\right]}{\nu}\right)^b \quad (53)$$

Using Eq. (53) in (41) we have for the present choice of $f(T)$

$$\dot{H} = -\frac{3a^{-\frac{2\nu}{\mu}} C_1 + \frac{\left(1 - \frac{a^{\frac{1}{n}} B}{K}\right)^n \left(a^{\frac{1}{n}} B - K\right)^{-n} 2F1\left[\frac{2n\nu}{\mu}, n, 1 + \frac{2n\nu}{\mu}, \frac{a^{\frac{1}{n}} B}{K}\right]}{\nu}}{2b} \quad (54)$$

As we are considering new holographic polytropic dark energy in $f(T)$ gravity, we can consider equality of Eqs. (54) and (52) from which we can express the integration constant C_1 as

$$C_1 = \frac{a^{\frac{2\nu}{\mu}} \left(a^{\frac{1}{n}} B - K\right)^{-n} \left(2b\nu + \left(1 - \frac{a^{\frac{1}{n}} B}{K}\right)^n (3\mu - 2b\nu) 2F1\left[\frac{2n\nu}{\mu}, n, 1 + \frac{2n\nu}{\mu}, \frac{a^{\frac{1}{n}} B}{K}\right]\right)}{3\nu(-3\mu + 2b\nu)} \quad (55)$$

As Eq. (55) is used in (51) the H^2 reduces to

$$H^2 = -\frac{2b \left(a^{\frac{1}{n}} B - K\right)^{-n}}{9\mu - 6b\nu} \quad (56)$$

and hence

$$\dot{H} = \frac{a^{\frac{1}{n}} b B \left(a^{\frac{1}{n}} B - K\right)^{-1-n}}{9\mu - 6b\nu} \quad (57)$$

Subsequently, effective torsion EoS and deceleration parameters become

$$w_T = -1 + \frac{a^{\frac{1}{n}} b B \left(4 + \alpha \left(\frac{b \left(a^{\frac{1}{n}} B - K\right)^{-n}}{-3\mu + 2b\nu}\right)^b \left(-2^{3+2b} b + \left(a^{\frac{1}{n}} B - K\right)^n (-34^b \mu + 2^{1+2b} b \nu)\right)\right)}{3 \left(a^{\frac{1}{n}} B - K\right) \left(4b + \left(a^{\frac{1}{n}} B - K\right)^n \alpha \left(\frac{b \left(a^{\frac{1}{n}} B - K\right)^{-n}}{-3\mu + 2b\nu}\right)^b (34^b \mu + 2^{1+2b} b (-3\mu + (-1 + 2b)\nu))\right)} \quad (58)$$

$$q_T = \frac{4 - \frac{3}{b} + \frac{16b \left(a^{\frac{1}{n}} B - K\right)^{-n}}{-3\mu + 2b\nu}}{2(-1 + 2b)} \quad (59)$$

$$w_{tot} = -1 + \frac{4a^{\frac{1}{n}}B + \left(a^{\frac{1}{n}}(34^b - 74^bb + 2^{1+2b}b^2)B - 34^bK + 32^{1+2b}bK\right) \alpha \left(\frac{b(a^{\frac{1}{n}}B-K)^{-n}}{-3\mu+2b\nu}\right)^{-1+b}}{12\left(a^{\frac{1}{n}}B - K\right)} \quad (60)$$

In this framework Eqs.(44) and (45) take the form

$$r = \frac{\left(4 - \frac{3}{b} + \frac{16b(a^{\frac{1}{n}}B-K)^{-n}}{-3\mu+2b\nu}\right) \left(3 - \frac{3}{b} + b\left(2 + \frac{16(a^{\frac{1}{n}}B-K)^{-n}}{-3\mu+2b\nu}\right)\right)}{2(1-2b)^2} \quad (61)$$

$$s = \frac{2 - \frac{3}{b} + b\left(4 + \frac{16(a^{\frac{1}{n}}B-K)^{-n}}{-3\mu+2b\nu}\right)}{3(-1+2b)} \quad (62)$$

and the other cosmographic parameter j (jerk parameter) (using Eq. (15)) takes the form

$$j = \frac{1}{2} \left(-4 + \frac{a^{\frac{1}{n}}B \left(K + a^{\frac{1}{n}}Bn\right)}{\left(-a^{\frac{1}{n}}B + K\right)^2 n} + \frac{3 \left(-4 + \frac{3}{b} + \frac{16b(a^{\frac{1}{n}}B-K)^{-n}}{3\mu-2b\nu}\right)}{-1+2b} \right) \quad (63)$$

In Figure 6, $f(T)$ is plotted against T and it is observed that $f(T) \rightarrow -\infty$ as $T \rightarrow 0$. The effective torsion parameter is plotted in Figure 7 and it is palpable that $w_T < -1$ i.e. behaves like phantom. The deceleration parameter plotted in Figure 8 shows an ever accelerating universe. The $w_{tot} < -1$ i.e. behaves like phantom as seen in Figure 9. The statefinders as obtained in Eqs. (61) and (62) are plotted in Figure 10 and the $\{r - s\}$ trajectory attains the Λ CDM point i.e. $\{r = 1, s = 0\}$. However, unlike the previous model the dust phase is not apparently attained by the statefinder trajectory.

Exponential model

We consider exponential $f(T)$ gravity [61]

$$f(T) = \delta \exp(\xi T) \quad (64)$$

Subsequently, using $T = -6H^2$ in Eq. (64), where H^2 is as obtained in Eq.(51), and thereafter using (32) we have the dark matter density of the universe as a function of a for present choice of

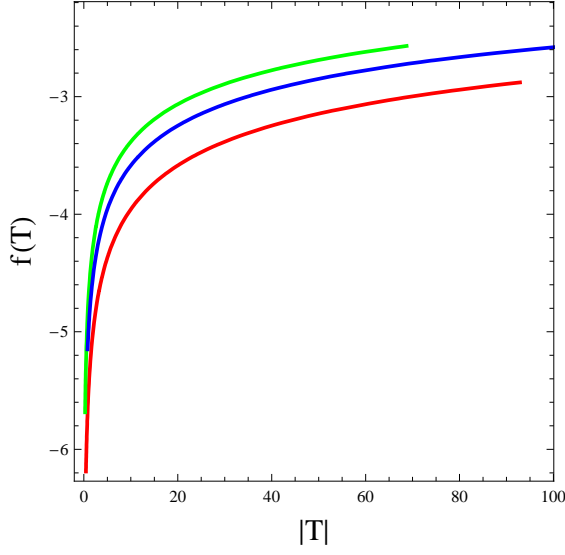
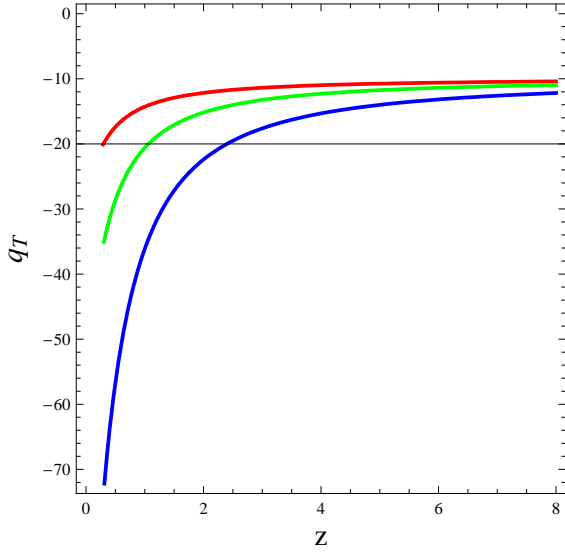
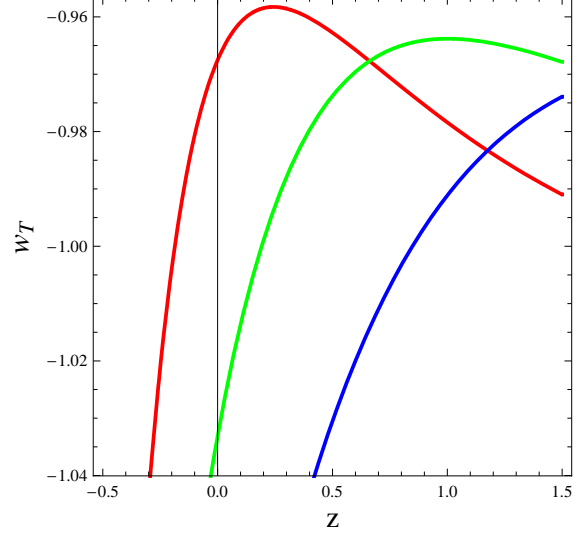
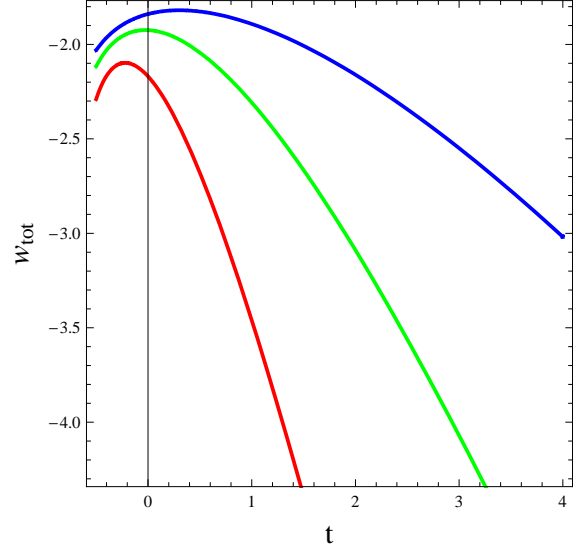
FIG. 6: Plot of $f(T)$ based on reconstructed H .FIG. 8: Deceleration parameter q_T for the Bengochea and Ferraro model.

FIG. 7: Effective torsion EoS parameter for the Bengochea and Ferraro model.

FIG. 9: Plot of w_{tot} as in Eq. (60).

f as

$$\rho_m = \frac{1}{2\nu} a^{-\frac{2\nu}{\mu}} e^{\left(-6a^{-\frac{2\nu}{\mu}} C_1 \xi - \frac{2 \left(1 - \frac{a^{\frac{1}{n}} B}{K} \right)^n \left(a^{\frac{1}{n}} B - K \right)^{-n} \xi {}_2F_1 \left[\frac{2n\nu}{\mu}, n, 1 + \frac{2n\nu}{\mu}, \frac{a^{\frac{1}{n}} B}{K} \right]}{\nu} \right)} \left(a^{\frac{1}{n}} B - K \right)^{-n} \times$$

$$\delta \left(\left(a^{\frac{1}{n}} B - K \right)^n \nu \left(a^{\frac{2\nu}{\mu}} + 12C_1 \xi \right) + 4a^{\frac{2\nu}{\mu}} \left(1 - \frac{a^{\frac{1}{n}} B}{K} \right)^n \xi {}_2F_1 \left[\frac{2n\nu}{\mu}, n, 1 + \frac{2n\nu}{\mu}, \frac{a^{\frac{1}{n}} B}{K} \right] \right) \quad (65)$$

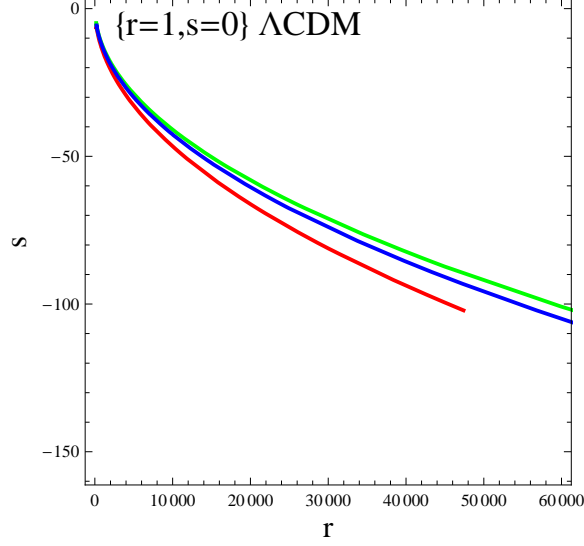


FIG. 10: Statefinder parameters for the choice of $f(T) = \alpha(-T)^b$.

Using Eq. (65) in (41) we have for the present choice of $f(T)$

$$\dot{H} = \frac{\left(a^{\frac{1}{n}}B - K\right)^n \nu \left(a^{\frac{2\nu}{\mu}} + 12C_1\xi\right) + 4a^{\frac{2\nu}{\mu}} \left(1 - \frac{a^{\frac{1}{n}}B}{K}\right)^n \xi {}_2F_1\left[\frac{2n\nu}{\mu}, n, 1 + \frac{2n\nu}{\mu}, \frac{a^{\frac{1}{n}}B}{K}\right]}{4\xi \left(-\left(a^{\frac{1}{n}}B - K\right)^n \nu \left(a^{\frac{2\nu}{\mu}} - 12C_1\xi\right) + 4a^{\frac{2\nu}{\mu}} \left(1 - \frac{a^{\frac{1}{n}}B}{K}\right)^n \xi {}_2F_1\left[\frac{2n\nu}{\mu}, n, 1 + \frac{2n\nu}{\mu}, \frac{a^{\frac{1}{n}}B}{K}\right]\right)} \quad (66)$$

Considering equality of Eqs. (54) and (66) we can express C_1 as

$$C_1 = \frac{1}{24\nu^2\xi^2} \left(a^{\frac{1}{n}}B - K\right)^{-2n} \left(\left(a^{\frac{4\nu}{\mu}} \left(a^{\frac{1}{n}}B - K\right)^{2n} \nu^2 \xi^2 \left(\left(a^{\frac{1}{n}}B - K\right)^{2n} \times \right. \right. \right. \\ \left. \left. \left(9\mu^2 - 18\mu\nu + \nu^2\right) - 8 \left(a^{\frac{1}{n}}B - K\right)^n (3\mu + \nu)\xi + 16\xi^2 \right)^{1/2} + a^{\frac{2\nu}{\mu}} \left(a^{\frac{1}{n}}B - K\right)^n \nu \xi \times \right. \\ \left. \left(\left(a^{\frac{1}{n}}B - K\right)^n (-3\mu + \nu) + 4\xi - 8 \left(1 - \frac{a^{\frac{1}{n}}B}{K}\right)^n \xi {}_2F_1\left[\frac{2n\nu}{\mu}, n, 1 + \frac{2n\nu}{\mu}, \frac{a^{\frac{1}{n}}B}{K}\right] \right) \right) \quad (67)$$

that finally leads to

$$\dot{H} = \left(a^{\frac{1}{n}}B \left(a^{\frac{1}{n}}B - K\right)^{-1-n} \left(a^{\frac{2\nu}{\mu}} \left(a^{\frac{1}{n}}B - K\right)^n \nu \left(\left(a^{\frac{1}{n}}B - K\right)^n (3\mu + \nu) - 4\xi \right) \xi \right. \right. \\ \left. \left. - \sqrt{a^{\frac{4\nu}{\mu}} \left(a^{\frac{1}{n}}B - K\right)^{2n} \nu^2 \xi^2 \left(\left(a^{\frac{1}{n}}B - K\right)^{2n} (9\mu^2 - 18\mu\nu + \nu^2) - 8 \left(a^{\frac{1}{n}}B - K\right)^n (3\mu + \nu)\xi + 16\xi^2 \right)} \right) \right) \\ \left(12\nu \sqrt{a^{\frac{4\nu}{\mu}} \left(a^{\frac{1}{n}}B - K\right)^{2n} \nu^2 \xi^2 \left(\left(a^{\frac{1}{n}}B - K\right)^{2n} (9\mu^2 - 18\mu\nu + \nu^2) - 8 \left(a^{\frac{1}{n}}B - K\right)^n (3\mu + \nu)\xi + 16\xi^2 \right)} \right)^{-1} \quad (68)$$

Fig. 11 shows that $f(T)$ is decreasing with increase in T . It is also observed that after certain stage $f(T)$ is behaving asymptotically. So, this behavior is in contrary to what happened in the last two models. Effective torsion parameter w_T displayed in Fig. 12 behaves like phantom and

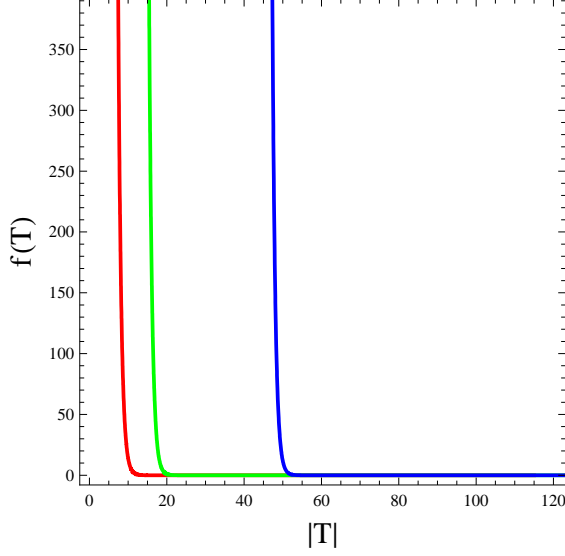


FIG. 11: Reconstructed $f(T)$ for the exponential model and we see that $f(T)$ becomes a decreasing function of T .

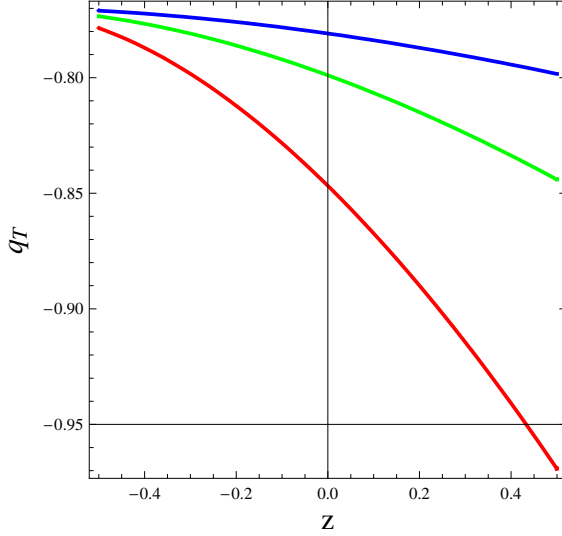


FIG. 13: Deceleration parameter using Eq. (68) in Eq. (39).

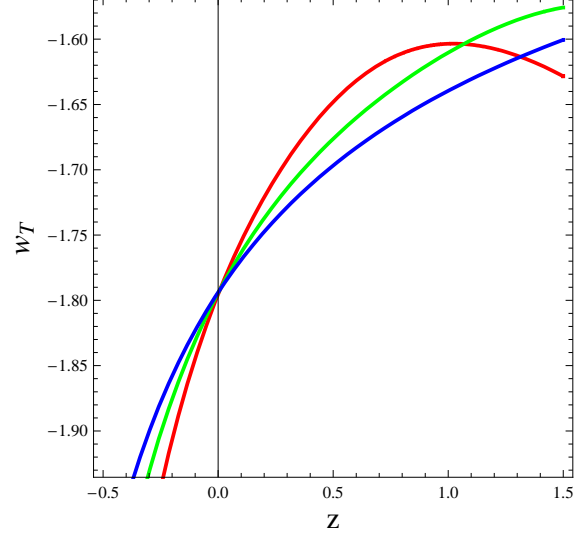


FIG. 12: Effective torsion EoS parameter based on reconstructed \dot{H} in Eq. (68).

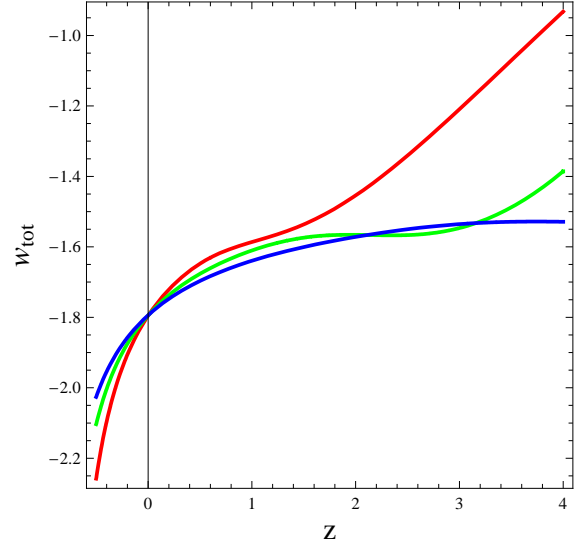


FIG. 14: Plot of w_{tot} using Eq. (68) in Eq. (43).

deceleration parameter displayed in Fig. 13 makes apparent an ever-accelerating universe. For $n = 6$ (red line), the w_{total} crosses phantom-divide at $z \approx 3.8$ (Fig. 14). However, for $n = 8$ and 10, w_{total} stays below the phantom-divide. The statefinder parameters $\{r, s\}$, when plotted in Fig. 15, is found to reach $\{r = 1, s = 0\}_{\Lambda CDM}$, but can not effectively go beyond it.

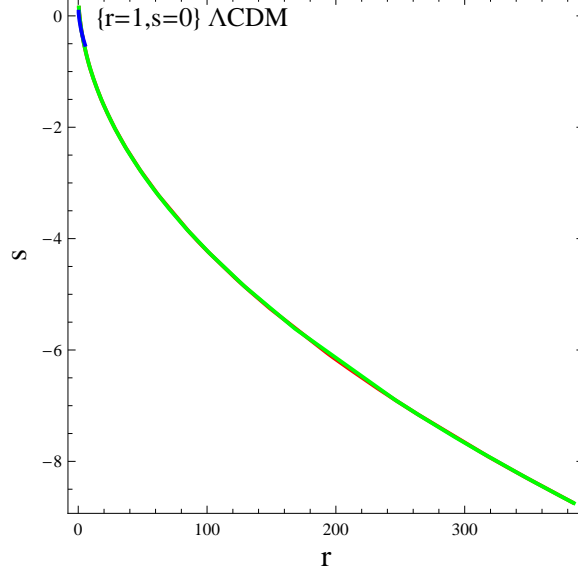


FIG. 15: Statefinder parameters for the choice of $f(T) = \delta \exp(\xi T)$.

C. Comparison with Observational

By implying different combination of observational schemes at 95% confidence level, Ade et al. [63] (Planck data) provided the following constraints for EoS

$$\begin{aligned}
 w_{DE} &= -1.13^{+0.24}_{-0.25} && (\text{Planck+WP+BAO}), \\
 w_{DE} &= -1.09 \pm 0.17, && (\text{Planck+WP+Union 2.1}) \\
 w_{DE} &= -1.13^{+0.13}_{-0.14}, && (\text{Planck+WP+SNLS}), \\
 w_{DE} &= -1.24^{+0.18}_{-0.19}, && (\text{Planck+WP+}H_0).
 \end{aligned}$$

The trajectories of EoS parameter also favor the following nine-year WMAP observational data

$$\begin{aligned}
 w_{DE} &= -1.073^{+0.090}_{-0.089} && (\text{WMAP+eCMB+BAO+}H_0), \\
 w_{DE} &= -1.084 \pm 0.063, && (\text{WMAP+eCMB+BAO+}H_0+\text{SNe}).
 \end{aligned}$$

It is interesting to mention here that the ranges of EoS parameter for both cases lie within these observational constraints.

III. STABILITY

The stability analysis of under consideration models in the present framework is being discussed in this section. For this purpose, we consider squared speed of sound which has the following

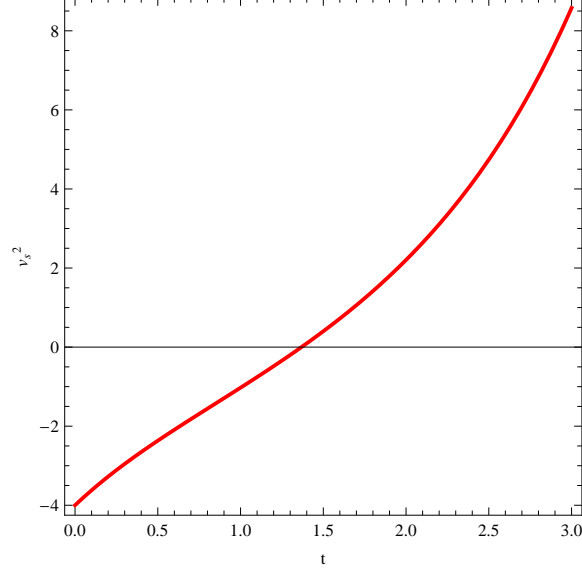


FIG. 16: Plot of Squared speed of sound with specific form of H .

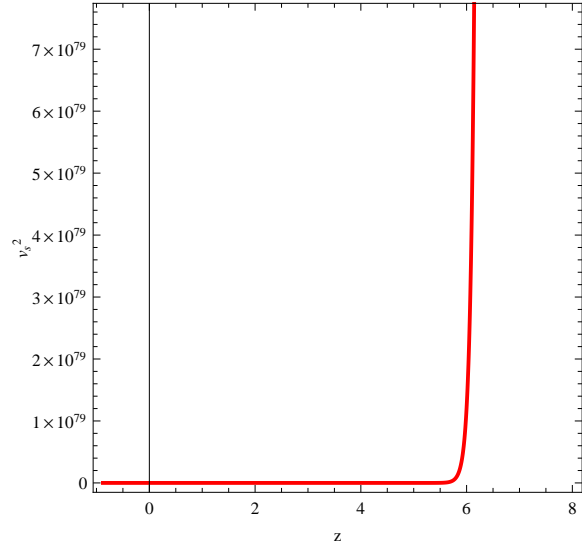


FIG. 17: Plot of Squared speed of sound for power-law form of $f(T)$.

expression

$$v_s^2 = \frac{\dot{p}_T}{\dot{\rho}_T}. \quad (69)$$

The sign of this parameter is very important in order to analyze the stability of model. This depicts the stable behavior for positive v_s^2 while its negativity expresses instability of the under consideration model. Inserting corresponding expressions and after some calculations, we can obtain squared speed of sound for all cases. We draw the graphs versus t for $n = 6$ in each case taking same values for the parameters to discuss the stability of the reconstructed $f(T)$ model. We

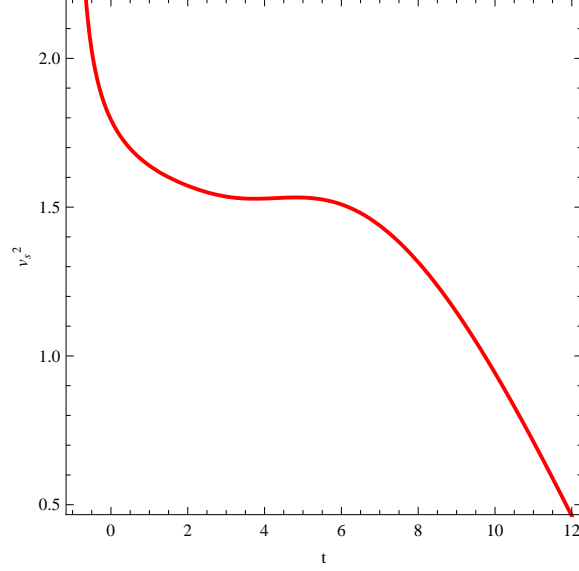


FIG. 18: Plot of Squared speed of sound for exponential form of $f(T)$.

provide a discussion about stability in each case in the following.

- **With a specific choice of H :**

Figure 16 represents the behavior of v_s^2 versus t for the particular choice of H . The graph shows unstable behavior initially but for a period $t < 1.4$. After this interval of time, squared speed of sound parameter maintain increasing behavior and becomes positive expressing stability of the model.

- **Without any choice of H :**

In this case, squared speed of sound shows increasing and positive behavior which exhibits the stability of the reconstructed model. The corresponding plot is given in Figure 17.

- **Exponential Model:**

Taking into account the case of exponential model, we plot the squared speed of sound parameter versus t as shown in Figure 18. The v_s^2 represents positively decreasing behavior establishing stability of the reconstructed model in this case throughout the time interval.

IV. CONCLUDING REMARKS

In the present work we have new holographically reconstructed the polytropic dark energy and this kind of holographic reconstruction of other dark energy models are already reported in [55–58]. Viewing $f(T)$ as an effective description of the underlying theory of DE, and considering the new

holographic polytropic dark energy as pointing in the direction of the underlying theory of DE, we have studied how the modified-gravity can describe the new holographic polytropic dark energy as effective theory of DE. This approach is largely motivated by [59, 60]. We have carried out this work through two approaches. In the first approach we have chosen H as $H = H_0 + \frac{H_1}{t}$ and consequently generated reconstructed $f(T)$ that is found to tend to 0 with T tending to 0 and thereby satisfying one of the sufficient conditions for a realistic model [60]. The effective torsion EoS parameter coming out of this reconstructed $f(T)$ is found to stay above -1 in contradiction to w_{tot} showing a clear transition from quintessence to phantom i.e. quintom. The deceleration parameter exhibits transition from decelerated to accelerated phase. The statefinder parameters $\{r, s\}$ could attain Λ CDM $\{r = 1, s = 0\}$ and could go beyond it. More particularly, it has been apparent from the statefinder plot that for finite r we have $s \rightarrow -\infty$ that indicates dust phase. Hence this reconstructed $f(T)$ model interpolates between dust and Λ CDM phase of the universe.

In the second approach instead of considering any particular form of the scale factor we have assumed a power-law and exponential solutions for $f(T)$ as proposed in [50] and [61] respectively. Under power-law solution we derived expressions for \dot{H} in terms of a . Thereafter we derived effective torsion EoS and deceleration parameters and also the statefinder parameters. For this reconstructed H , the $f(T)$ has been found to behave like the earlier approach that is tending to 0 as T tends to 0. As plotted against redshift z , the effective torsion EoS as well as w_{tot} are found to exhibit phantom-like behavior. The deceleration parameter is found to stay negative i.e. exhibited accelerated expansion. Although the statefinder plot could attain Λ CDM, no clear attainment of dust phase is apparent. Under exponential solution of $f(T)$ we derived expressions for \dot{H} in terms of a and subsequently reconstructed f does not tend to 0 as T tends to 0 and hence it does not satisfy the sufficient condition for realistic model. The effective torsion equation of state parameter derived this way exhibited phantom-like behavior. However, w_{total} exhibits a transition from > -1 to < -1 for $n = 6$. We have discussed the stability of the model through squared speed of sound in all cases. We have obtained a large intervals where models behave like stable models. Cosmographic parameter j , based on Eqs. (48) and (63) plotted against t and z in Figs. 19 and 20 respectively show that for both reconstruction models with and without any choice of H the jerk parameter j is increasing gradually with evolution of the universe and remains positive throughout. This observation is somewhat consistent with the work of [62].

In view of the above, although both of the approaches are found to be somewhat consistent with expected cosmological consequences, the first approach could be stated to be more acceptable as it could show a transition from decelerated to accelerated expansion and could interpolate between

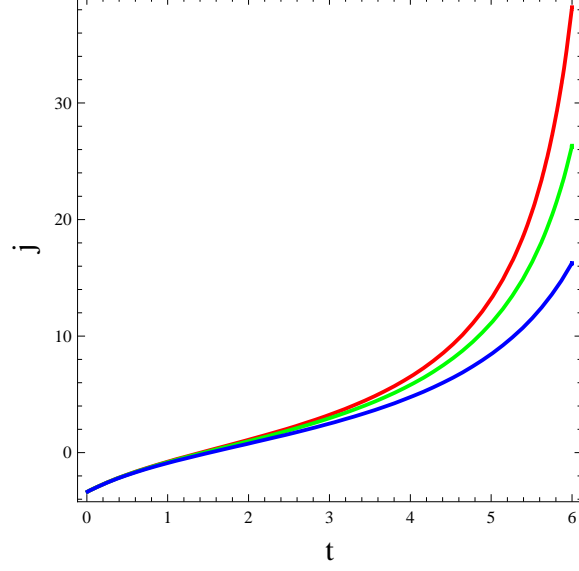
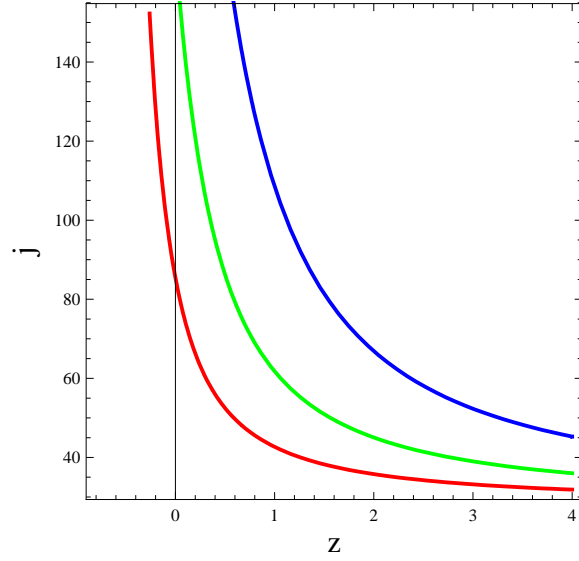


FIG. 19: Jerk parameter plot corresponding to Eq. (48).

FIG. 20: Jerk parameter plot against redshift z corresponding to Eq. (63).

dust and Λ CDM phase of the universe. Secondly, in the first approach, w_{total} transited from quintessence to phantom that is found to be consisted with the outcomes of [61], where cosmological evolutions of the equation of state for DE in $f(T)$ gravity was seen to have a transition of similar nature. However, one major difference between [61] and the present work lies in the fact that in [61] the equation of state parameter behaved like quintom irrespective of exponential, power-law or combined $f(T)$ gravity. Contrarily, in our present work, the equation of state parameter of holographic-polytropic gas DE does not necessarily exhibit quintom behavior.

V. ACKNOWLEDGEMENT

Constructive suggestions from the reviewers are thankfully acknowledged by the authors. Visiting associateship of IUCAA, Pune, India and financial support from DST, Govt of India under project grant no. SR/FTP/PS-167/2011 are acknowledged by SC.

-
- [1] Riess, A.G. et al.: *Astron. J.* **116**(1998)1009.
 - [2] Perlmutter, S. et al.: *Astrophys. J.* **517**(1999)565.
 - [3] Caldwell, R.R. and Doran, M.: *Phys. Rev. D* **69**(2004)103517.
 - [4] Koivisto, T. and Mota, D.F.: *Phys. Rev. D* **73**(2006)083502.
 - [5] Fedeli, C., Moscardini, L. and Bartelmann, M.: *Astron. Astrophys.* **500**(2009)667.
 - [6] E. J. Copeland, M. Sami, S. Tsujikawa, *Int. J. Mod. Phys. D*, **15**, 1753 (2006).
 - [7] K. Bamba, S. Capozziello, S. Nojiri, S. D. Odintsov, *Astrophys. Space Sci.*, **342**, 155 (2012).
 - [8] R. R. Caldwell, M. Kamionkowski, *Ann. Rev. Nucl. Part. Sci.* **59**, 397 (2009).
 - [9] S. Nojiri, S. D. Odintsov, *Phys. Rep.*, **505**, 59 (2011).
 - [10] V. Sahni, A. A. Starobinsky, *Int. J. Mod. Phys. D* **9**, 373 (2000).
 - [11] V. Sahni, A. A. Starobinsky, *Int. J. Mod. Phys. D* **15**, 2105 (2006).
 - [12] H. Motohashi, A. A. Starobinsky, J. Yokoyama, *Prog. Theor. Phys.* **123**, 887 (2010).
 - [13] P. J. E. Peebles, B. Ratra, *Rev. Mod. Phys.* **75**, 559 (2003).
 - [14] S. Nojiri, S. D. Odintsov, O. G. Gorbunova, *J. Phys. A: Math. Gen.* **39**, 6627 (2006).
 - [15] A. V. Astashenok, S. Nojiri, S. D. Odintsov, R. J. Scherrer, *Phys. Lett. B* **713**, 145 (2012).
 - [16] B. Gumjudpai, T. Naskar, M. Sami, S. Tsujikawa, *J. Cosmol. Astropart. Phys.* **06**, 007 (2005).
 - [17] E. Elizalde, S. Nojiri, S. D. Odintsov, *Phys. Rev. D* **70**, 043539 (2004).
 - [18] S. Nojiri, S. D. Odintsov, S. Tsujikawa, *Phys. Rev. D* **71**, 063004 (2005).
 - [19] H. Zhang, Z-H. Zhu, *Phys. Rev. D* **73**, 043518 (2006).
 - [20] K. Bamba, J. Matsumoto, S. Nojiri, *Phys. Rev. D* **85**, 084026 (2012).
 - [21] M. Forte, *Phys. Rev. D* **90**, 027302 (2014).
 - [22] Nojiri, S. and Odintsov, S.D.: *Int. J. Geom. Meth. Mod. Phys.* **4** 115 (2007).
 - [23] Nojiri, S. and Odintsov, S.D.: *Phys. Rept.* **505**, 59 (2011).
 - [24] Nojiri, S., Odintsov, S. D.: *Gen. Relativ. Gravit.* **38**, 1285 (2006).
 - [25] Nojiri, S., Odintsov, S. D.: *Phys. Lett. B* **631**, 1 (2005).
 - [26] Bamba, K., Nojiri, S. and Odintsov, S.D.: *Phys. Lett. B* **725**(2013)368.
 - [27] Bamba, K. et al.: *Astrophys. Space Sci.* **341**(2012)155.
 - [28] Bamba, K., Jamil, M., Momeni, D. and Myrzakulov, R.: *Astrophys. Space Sci.* **344**(2013)259.
 - [29] Daouda, M.H., Rodrigues, M.E. and Houndjo, M.J.S.: *Eur. Phys. J. C* **72**(2012)1893.

- [30] Setare, M.R. and Darabi, F.: Gen. Relativ. Gravit **44**(2012)2521.
- [31] S. Nojiri, S. D. Odintsov, Phys. Lett. B **716**, 377 (2012).
- [32] S. Nojiri, S. D. Odintsov, N. Shirai, J. Cosmol. Astropart. Phys. **1305**, 020 (2013).
- [33] K. Bamba, S. Nojiri, S. D. Odintsov, Report OCHA-PP-323 (2014).
- [34] Farooq, M.U., Jamil, M., Momeni, D. and Myrzakulov, R.: Can. J. Phys. **91**(2013)703.
- [35] Karami, K. and Abdolmaleki, A.: Res. Astron. Astrophys. **13**(2013)757.
- [36] Sharif, M. and Rani, S.: Astrophys. Space Sci. **345**(2013)217.
- [37] Sharif, M. and Rani, S.: Mod. Phys. Lett. A **29**(2014)1450015.
- [38] t'Hooft, G.: gr-qc/9310026.
- [39] Susskind, L.: J. Math. Phys. **36**(1995)6377.
- [40] Bekenstein, J.D.: Phys. Rev. D **7**(1973)2333.
- [41] Cohen, A., Kaplan, D. and Nelson, A.: Phys. Rev. Lett. **82**(1999)4971.
- [42] Li, M.: Phys. Lett. B **603**(2004)1.
- [43] Wei, H.: Commun. Theor. Phys. **52**(2009)743; Sheykhi, A. and Jamil, M.: Gen. Relativ. Gravit. **43**(2011)2661.
- [44] Karami, K. and Abdolmaleki, A.: J. Phys.: Conf. Ser. **375** 032009 (2012).
- [45] Sharif, M. and Rani, S.: Astrophys. Space Sci. **346**(2013)573.
- [46] Sharif, M. and Rani, S.: J. Exp. Theor. Phys. **119**(2014)75.
- [47] Sahni, V. et al.: J. Exp. Theor. Phys. Lett. **77**(2003)201.
- [48] A. Aviles, A. Bravetti, S. Capozziello, and O. Luongo Phys. Rev. D **87**, 064025 (2013).
- [49] S. Capozziello, O. Luongo, E. N. Saridakis, Phys. Rev. D, **91**, 124037 (2015).
- [50] G. R. Bengochea and R. Ferraro, Phys. Rev. D **79**, 124019 (2009).
- [51] K. Karami, S. Ghaffari, Phys. Lett. B **688**, 125 (2010).
- [52] K. Karami, S. Ghaffari, J. Fehri, Eur. Phys. J. C **64**, 85 (2009).
- [53] L. N. Granda, A. Oliveros, Phys. Lett. B **669**, 275 (2008).
- [54] S. Nojiri, S. D. Odintsov, Phys. Rev. D **74**, 086005 (2006).
- [55] K. Karami, J. Fehri, Phys. Lett. B **684**, 61 (2010).
- [56] U. Debnath, Eur. Phys. J. Plus **129**, 272 (2014).
- [57] A. Sheykhi, Phys. Rev. D **84**, 107302 (2011).
- [58] S. Chattopadhyay, A. Pasqua, M. Khurshudyan, Eur. Phys. J. C **74**, 3080 (2014).
- [59] W. Yang, Y. Wu, L. Song, Y. Su, J. Li, D. Zhang, X. Wang, Mod. Phys. Lett. A **26**, 191 (2011).
- [60] M. R. Setare, Int. J. Mod. Phys. D, **17**, 2219 (2008).
- [61] K. Bamba, C-Q. Geng, C-C. Lee, L-W. Luo, JCAP **021** 1101 (2011).
- [62] S. Pan, S. Chakraborty, Int. J. Mod. Phys. D **23**, 1450092 (2014).
- [63] Ade, P.A.R., et al.: Astronom. Astrophys. **571**(2014)A16.

